The Astrophysical Journal Letters, 789:L2 (7pp), 2014 July 1 doi:10.1088/2041-8205/789/1/L2

THE NEAREST HIGH-VELOCITY STARS REVEALED BY LAMOST DATA RELEASE 1

Jing Zhong[1], Li Chen[1], Chao Liu[2], Richard de Grijs[3], Jinliang Hou[1], Shiyin Shen[1], Zhengyi Shao[1], Jing Li[1], Ali Luo[2], Jianrong Shi[2], Haotong Zhang[2], Ming Yang[2], Licai Deng[2], Ge Jin[4], Yong Zhang[5], Yonghui Hou[5], and Zhenchao Zhang[5]

[1] Key Laboratory for Research in Galaxies and Cosmology, Shanghai Astronomical Observatory, Chinese Academy of Sciences, 80 Nandan Road, Shanghai 200030, China; jzhong@shao.ac.cn

[2] Key Laboratory of Optical Astronomy, National Astronomical Observatories, Chinese Academy of Sciences, Datun Road 20A, Beijing 100012, China

[3] Kavli Institute for Astronomy and Astrophysics and Department of Astronomy, Peking University, Yi He Yuan Lu 5, Hai Dian District, Beijing 100871, China

[4] University of Science and Technology of China, Hefei 230026, China

[5] Nanjing Institute of Astronomical Optics and Technology, National Astronomical Observatories, Chinese Academy of Sciences, Nanjing 210042, China

Received 2014 February 13; accepted 2014 May 28; published 2014 June 10

ABSTRACT

We report the discovery of 28 candidate high-velocity stars (HVSs) at heliocentric distances of less than 3 kpc, based on the Large Sky Area Multi-Object Fiber Spectroscopic Telescope (LAMOST) Data Release 1. Our sample of HVS candidates covers a much broader color range than the equivalent ranges discussed in previous studies and comprises the first and largest sample of HVSs in the immediate solar neighborhood, at heliocentric distances less than 1–3 kpc. The observed as well as the derived parameters for all candidates are sufficiently accurate to allow us to ascertain their nature as genuine HVSs, of which a subset of 12 objects represents the most promising candidates. Our results also highlight the great potential of discovering statistically large numbers of HVSs of different spectral types in LAMOST survey data. This will ultimately enable us to achieve a better understanding of the nature of Galactic HVSs and their ejection mechanisms, and to constrain the structure of the Galaxy.

Key words: astrometry – Galaxy: halo – Galaxy: structure – stars: kinematics and dynamics – surveys

1. INTRODUCTION

High-velocity stars (HVSs) move sufficiently fast so that they can escape from the Galaxy's gravitational pull. They may have attained their high velocities through three-body interactions, for instance, among binary systems in star clusters (e.g., Leonard 1991; Moyano Loyola & Hurley 2013 and references therein) or with the supermassive black hole in the Galactic center (GC; e.g., Hills 1988; Yu & Tremaine 2003; Brown et al. 2005). While this latter formation mechanism is thought to be very promising, other HVS ejection scenarios are possible, such as those involving close encounters of single stars with binary black holes (Yu & Tremaine 2003) or the disruption of stellar binaries in the Galactic disk (Wang & Han 2009; Napiwotzki & Silva 2012).

Until recently, most confirmed and potential HVSs had been identified as early-type stars located at Galactocentric distances greater than 20 kpc. At present, dozens of confirmed HVSs are known in the Milky Way (Brown et al. 2005, 2009, 2012; see also Tillich et al. 2009, 2010), most of which are massive B-type stars. To distinguish among HVS ejection mechanisms and place firm constraints on the origin of their parent population, construction of larger HVS candidate samples spanning a much wider range of spectral types is imperative. Based on Sloan Digital Sky Survey (SDSS) data, Kollmeier et al. (2009, 2010) attempted to find metal-rich, old-population HVS stars (mainly F/G stellar types) that had been ejected from the GC. However, their non-detection of such old-population ejectees only places a limit on the rate of ejection, which suggests that the stellar mass function in the GC may be top- instead of bottom-heavy, or alternatively that the supermassive black hole ejection mechanism often involved for the ejection of lower-mass stars is less effective than expected. Recently, Li et al. (2012) reported the discovery of 13 F-type HVSs, located at distances ranging from 3 kpc to 10 kpc. Palladino et al. (2014) identified 20 high-velocity G- and K-dwarf candidates, discovered in the Sloan Extension for Galactic Understanding and Exploration sample, most of which are located far beyond the solar neighborhood (at distances of 3–6 kpc). The first HVS discovered in the Large Sky Area Multi-Object Fiber Spectroscopic Telescope (LAMOST) survey, a B-type star characterized by a galactocentric radial-velocity (RV) component of approximately 477 km s^{-1} and a heliocentric distance of ∼13 kpc, was recently reported by Zheng et al. (2014).

Here we report the discovery of 28 solar-neighborhood HVS candidates based on the LAMOST Data Release 1 (DR1). All candidates have velocities, with respect to the Galactic rest frame, in excess of 300 km s^{-1}; 12 objects move faster than 400 km s^{-1}. Our HVS candidate sample covers a much more extended color range than addressed in previous studies, while most targets are located at heliocentric distances within 3 kpc (some even within 1 kpc). Our sample comprises the first large HVS sample in the immediate solar neighborhood. As a consequence, it is of great importance for investigating the various HVS ejection mechanisms, which may be more complex than previously thought (e.g., Palladino et al. 2014).

This Letter is organized as follows. In Section 2, a brief description of the LAMOST survey data and our candidate selection is presented. We discuss distance estimates to our HVS candidates and derive their kinematic properties in Section 3. The key results are presented in Section 4.

2. LAMOST SURVEY DATA AND HVS CANDIDATE SELECTION

2.1. LAMOST DR1 Data

LAMOST—the "Guoshoujing telescope"—is a Schmidt telescope with an effective aperture of 4 m. It is equipped with 4000 fibers that can be deployed across a 5° (diameter) field of view,

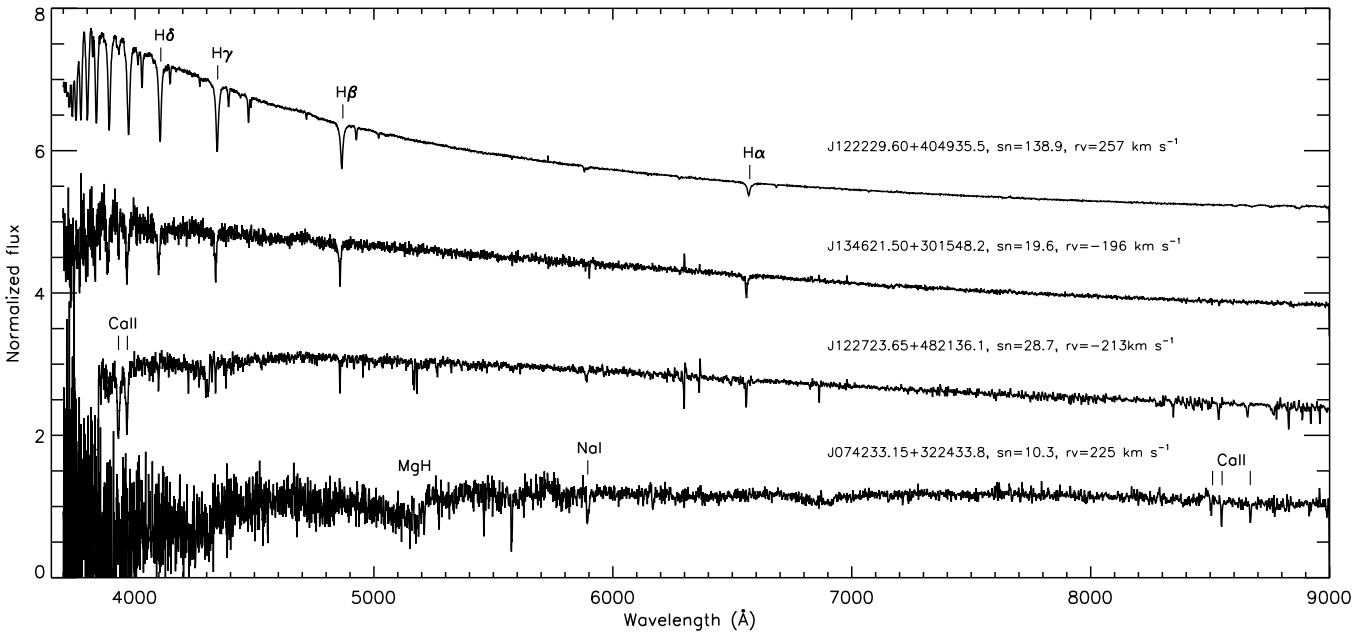

Figure 1. Typical spectral sequence representative of our HVS candidates. A number of different absorption lines are used for measuring the average wavelength shift and computing the RVs. The LAMOST designation, S/N, and RV are shown above the respective spectrum.

with a spectral resolution of $R \simeq 1800$ over the wavelength range from 3800 Å to 9100 Å (Cui et al. 2012; Zhao et al. 2012).

DR1, based on a year of pilot operations and the first season of official survey science, contains 1.7×10^6 spectra suitable for accurate RV measurements. Most of these spectra represent observations obtained as part of the LAMOST Experiment for Galactic Understanding and Exploration survey (Deng et al. 2012) aimed at unveiling the structure of the Milky Way. A subset of some 1.3 million spectra, mostly of bright ($r < 17$ mag) stars spanning a broad color range, are characterized by signal-to-noise ratios (S/N) greater than 5 in the SDSS g, r, and i filters. The sample selection criteria (see Carlin et al. 2012; Chen et al. 2012; Yang et al. 2012; Zhang et al. 2012) favor inclusion of nearby main-sequence stars, simply because of their preponderance along any line of sight.

2.2. HVS Candidate Selection

By 2013 March 20, regular LAMOST survey operations had observed and processed around one million stellar spectra. The standard reduction pipeline (Zhao et al. 2012) converts two-dimensional into one-dimensional (1D) spectra, applies flat-field corrections, combines the blue and red spectral ranges, and takes care of wavelength calibration and sky subtraction. The pipeline also provides stellar RVs based on cross correlation with the ELODIE library (Prugniel et al. 2007). Although the process of stellar parameter determination, including determination of the appropriate stellar surface gravities ($\log g$), effective temperatures ($T_{\rm eff}$), and metallicities ([Fe/H]), is still being refined, stellar RVs based on "good-quality spectra" (S/N > 5) are highly accurate (see Luo et al. 2012, where the quotes refer to verbatim text from that reference), with uncertainties of the order of 13 km s^{-1}.

For a systematic investigation of HVS candidates, we first selected the 14,650 stars in the LAMOST DR1 with absolute RV values greater than 200 km s^{-1}. Next, to derive three-dimensional (space) velocities, we identified the 6148 targets for which we had both proper motions—from the Fourth U.S. Naval Observatory CCD Astrograph Catalog (UCAC4)—and SDSS DR9 photometry ($r < 18.5$ mag) available, with sufficient S/N in both the g and i bands (S/N $\geqslant$ 6 and S/N $\geqslant$ 20, respectively). This resulted in an astrometric catalog containing 2600 candidates.

To derive photometric distances, we need reliable estimates of the stellar metallicities. Starting from our 2600 candidate HVSs, we further excluded stars for which either their LAMOST-based [Fe/H] values are not available or their SDSS colors fall outside either the $[0.2 < (g-r) < 0.6, 0.8 < (u-g) < 1.3]$ mag or $[0.1 < (r-i) < 1.6]$ mag ranges (Ivezić et al. 2008), where sufficiently accurate photometric metallicities can be derived. We subsequently selected the remaining 1800 candidates to calculate the preliminary stellar distances and space velocities in the Galactic rest frame ($V_{\rm gt}$). Upon imposing an additional selection criterion of $V_{\rm gt} > 300$ km s^{-1}, only approximately 200 candidates were left. We visually inspected this final subsample and calculated the equivalent widths of the Mgb (5180 Å), Hβ (4863 Å), and TiO lines (6150 Å) for each LAMOST spectrum. We next verified the stellar RVs in our sample catalog and excluded those spectra that were characterized by low S/N. The RVs resulting from such observations were insufficiently reliable because they lacked a sufficient number ($\geqslant$3) of spectral lines for calibration. We also excluded those spectra that more likely represented the characteristics of red giant stars according to the classification criteria derived by Liu et al. (2014). We finally obtained a HVS candidate sample containing 28 objects; see Table 1.

3. HVS CANDIDATE VERIFICATION

3.1. RV Verification

To verify the LAMOST RV results, we used the IRAF/`rv.rvidlines` package. Figure 1 shows four typical spectra representative of our sample objects. For early-type stars (top and second panels), we predominantly used the Balmer lines—Hα (6563 Å), Hβ, Hγ (4341 Å), and Hδ (4102 Å)—to compute the average wavelength shift and obtain the best-fitting RV; for late-type stars (third and bottom panels), we used other

Table 1
Basic Parameters of the 28 HVS Candidates

Designation	R.A. (deg)	Decl. (deg)	$\mu_\alpha \cos(\delta)$ (mas yr^{-1})	μ_δ (mas yr^{-1})	u (mag)	g (mag)	r (mag)	i (mag)	z (mag)	J (mag)	H (mag)	K_s (mag)	$W2$ (mag)	[Fe/H] (dex)	V_r^a (km s^{-1})	V_r^b (km s^{-1})	SpTy
J085819.90+150352.4	134.58293	15.064578	-21.8 ± 2.6	-54.3 ± 3.0	15.23	14.22	14.38	14.13	13.82	12.94	12.69	12.64	12.63	-1.11	428	415	A5
J092707.09+242752.9	141.77954	24.464709	-59.8 ± 8.5	-2.7 ± 8.0	17.17	16.18	15.83	15.90	15.67	14.90	14.58	14.50	14.40	-1.56	306	308	F5
J074233.15+322433.8	115.63816	32.409389	-156.0 ± 8.0	-353.0 ± 8.0	19.96	17.47	16.12	15.57	15.26	14.10	13.62	13.43	13.09	···	233	225	K7
J225922.58+262409.9	344.84410	26.402775	-49.3 ± 4.2	72.2 ± 4.5	16.19	15.26	14.96	14.84	14.81	14.04	13.70	13.64	13.62	···	-229	-220	B6
J115445.93+523520.3	178.69142	52.588984	56.3 ± 2.2	-76.4 ± 2.6	16.42	15.36	14.95	14.90	14.75	13.88	13.55	13.53	13.46	···	-228	-219	F2
J082932.48+282613.3	127.38536	28.437039	-196.0 ± 8.0	-395.0 ± 8.0	18.99	16.51	15.18	14.64	14.34	13.20	12.64	12.44	12.21	···	279	282	K7
J231232.05+265039.5	348.13358	26.844326	63.6 ± 2.9	14.6 ± 3.0	16.12	15.08	14.63	14.78	14.37	13.48	13.08	13.00	13.01	-0.70	-235	-196	F5
J135931.65+413121.6	209.88189	41.522689	-70.3 ± 2.8	-78.4 ± 3.7	16.47	15.47	15.11	14.96	14.93	14.11	13.75	13.66	13.70	···	261	244	F5
J134621.50+301548.2	206.58962	30.263401	-15.2 ± 3.9	-58.4 ± 4.2	16.56	15.66	15.45	15.37	15.37	14.59	14.37	14.37	14.21	···	-244	-196	A0
J110208.65+575200.2	165.53608	57.866742	70.6 ± 1.9	-84.0 ± 1.6	14.67	13.42	14.61	12.95	13.24	11.96	11.65	11.63	11.61	-1.16	-219	-227	A0
J224145.15+292428.4	340.43813	29.407892	-15.3 ± 7.2	-60.4 ± 10.0	16.03	15.09	14.88	14.78	14.76	13.99	13.72	13.72	13.73	···	-220	-210	A0
J124020.02+453259.6	190.08345	45.549896	26.2 ± 2.6	-52.8 ± 2.6	16.32	15.42	15.15	15.05	15.06	14.34	14.01	14.02	13.95	-1.30	-219	-195	A0
J123134.97+424736.1	187.89571	42.793379	17.2 ± 2.9	-49.2 ± 2.6	16.83	15.89	15.57	15.46	15.44	14.59	14.31	14.18	14.36	-1.35	-254	-266	F0
J094122.37-000822.2	145.34323	-0.139505	-46.5 ± 4.4	-67.6 ± 4.6	16.54	15.54	15.23	15.07	15.05	14.20	14.01	13.91	13.85	-1.62	430	426	F0
J073050.71+293212.6	112.71130	29.536856	21.9 ± 3.2	-77.7 ± 2.9	15.85	14.86	14.52	14.40	14.37	13.56	13.21	13.22	13.16	-1.20	-309	-291	F5
J123641.48+443715.9	189.17285	44.621092	-23.7 ± 3.2	-55.6 ± 3.0	17.22	16.35	16.07	15.95	15.95	15.12	14.90	14.95	14.79	-1.79	-257	-259	F0
J085623.74+211322.3	134.09893	21.222872	-60.0 ± 3.4	-47.3 ± 2.6	15.09	14.15	13.81	13.88	13.77	12.83	12.50	12.51	12.48	-1.46	223	235	F0
J173650.63+060814.4	264.21098	6.1373510	-30.9 ± 18.7	-15.5 ± 7.0	16.57	15.25	14.73	14.50	14.39	13.44	13.03	12.99	12.95	-1.51	-436	-416	F5
J224207.91+072808.3	340.53297	7.4689990	60.2 ± 2.3	-42.7 ± 2.6	16.06	15.28	16.33	14.60	14.43	13.50	13.18	13.24	13.15	-2.18	-462	-436	A0
J091849.92-005331.5	139.70801	-0.892091	-45.3 ± 3.2	-85.7 ± 3.0	14.79	13.91	13.73	13.47	13.42	12.48	12.24	12.20	12.15	-1.81	453	465	A5
J122723.65+482136.1	186.84858	48.360029	15.3 ± 3.5	-88.2 ± 3.7	17.04	15.88	15.44	15.28	15.19	14.36	13.96	13.84	13.89	-1.11	-209	-213	G0
J124330.95+423119.9	190.87898	42.522216	-25.4 ± 2.5	-55.5 ± 2.5	16.74	15.90	15.64	15.56	15.53	14.85	14.56	14.46	14.55	-2.20	-229	-263	A0
J121437.93+542522.9	183.65808	54.423052	17.0 ± 3.8	-62.6 ± 4.0	15.93	14.98	14.72	14.63	14.65	13.82	13.59	13.54	13.57	···	-203	-197	A0
J212028.30-013323.4	320.11794	-1.556502	51.2 ± 3.8	-47.0 ± 4.0	16.87	15.99	15.67	15.54	15.53	14.76	14.36	14.54	14.30	-2.18	-338	-311	F0
J080608.76+063349.8	121.53652	6.5638360	14.2 ± 4.6	-20.4 ± 5.1	16.84	15.91	15.65	15.57	15.54	14.84	14.50	14.43	14.64	-1.25	427	423	A0
J065436.50+170313.8	103.64375	17.053856	-1.4 ± 2.1	-16.0 ± 2.3	15.57	14.05	13.55	13.40	13.60	12.31	11.98	11.91	11.84	-1.23	290	307	F9
J102757.74+090030.0	156.99059	9.008337	-160.0 ± 8.0	-35.0 ± 8.0	15.67	14.50	14.03	14.06	13.73	12.28	12.29	12.80	12.38	···	293	314	G2
J120758.23+093231.9	181.99265	9.542214	-100.0 ± 8.0	-137.0 ± 8.0	15.83	14.60	14.00	14.24	13.65	12.04	12.07	12.65	12.10	-1.55	215	214	G2

Notes. $\mu_\alpha \cos(\delta)$ and μ_δ were taken from the UCAC4; u, g, r, i, and z are from SDSS photometry; J, H, and K_s are taken from the Two Micron All-Sky Survey (2MASS) catalog; $W2$ is from the *WISE* catalog; V_r^a was obtained from the LAMOST 1D pipeline, while V_r^b is based on our IRAF reduction; SpTy is the spectral type from the LAMOST 1D pipeline.

Table 2
Spatial Positions and Kinematic Parameters of the 28 HVS Candidates

Name	Designation	R.A. (deg)	Decl. (deg)	A_V (mag)	$D_\odot$ (kpc)	r_{gc} (kpc)	x (kpc)	y (kpc)	z (kpc)	V_x (km s^{-1})	V_y (km s^{-1})	V_z (km s^{-1})	V_{gt} (km s^{-1})
LMST_HVS1	J085819.90+150352.4	134.58293	15.064578	0.062	3.3	10.5	−10.3	−1.5	1.9	−227 ± 7	−705 ± 42	−288 ± 6	795 ± 35
LMST_HVS2	J092707.09+242752.9	141.77954	24.464709	0.085	2.3	9.6	−9.5	−0.6	1.6	−655 ± 10	92 ± 79	−233 ± 45	707 ± 7
LMST_HVS3	J074233.15+322433.8	115.63816	32.409389	0.104	0.4	8.4	−8.3	−0.0	0.1	−329 ± 18	−412 ± 51	−382 ± 24	652 ± 56
LMST_HVS4	J225922.58+262409.9	344.84410	26.402775	0.256	0.9	8.1	−8.0	0.8	−0.5	46 ± 26	248 ± 34	470 ± 36	535 ± 46
LMST_HVS5	J115445.93+523520.3	178.69142	52.588984	0.051	1.1	8.4	−8.4	0.3	1.0	492 ± 41	−50 ± 2	48 ± 31	497 ± 43
LMST_HVS6	J082932.48+282613.3	127.38536	28.437039	0.085	0.2	8.2	−8.2	−0.0	0.1	−311 ± 15	−318 ± 42	−177 ± 15	480 ± 43
LMST_HVS7	J231232.05+265039.5	348.13358	26.844326	0.171	1.6	8.3	−8.1	1.4	−0.8	−465 ± 82	−55 ± 0	10 ± 6	469 ± 81
LMST_HVS8	J135931.65+413121.6	209.88189	41.522689	0.033	1.0	8.0	−7.9	0.3	0.9	31 ± 0	−164 ± 22	409 ± 22	443 ± 28
LMST_HVS9	J134621.50+301548.2	206.58962	30.263401	0.045	2.0	7.9	−7.7	0.3	2.0	238 ± 29	−326 ± 8	−129 ± 8	425 ± 11
LMST_HVS10	J110208.65+575200.2	165.53608	57.866742	0.024	0.8	8.4	−8.4	0.2	0.6	409 ± 28	−56 ± 9	85 ± 37	423 ± 35
LMST_HVS11	J224145.15+292428.4	340.43813	29.407892	0.192	1.4	8.1	−8.0	1.3	−0.6	326 ± 49	−76 ± 11	−171 ± 5	377 ± 43
LMST_HVS12	J124020.02+453259.6	190.08345	45.549896	0.042	1.4	8.4	−8.2	0.3	1.3	373 ± 36	−10 ± 7	−58 ± 19	379 ± 32
LMST_HVS13	J123134.97+424736.1	187.89571	42.793379	0.073	1.3	8.3	−8.2	0.2	1.3	316 ± 30	−32 ± 6	−152 ± 18	354 ± 18
LMST_HVS14	J094122.37-000822.2	145.34323	−0.139505	0.167	0.9	8.4	−8.4	−0.6	0.5	−189 ± 2	−291 ± 16	−10 ± 4	348 ± 14
LMST_HVS15	J073050.71+293212.6	112.71130	29.536856	0.189	0.8	8.7	−8.7	−0.1	0.2	321 ± 3	−24 ± 25	−117 ± 16	344 ± 7
LMST_HVS16	J123641.48+443715.9	189.17285	44.621092	0.045	1.7	8.5	−8.3	0.3	1.6	116 ± 13	−294 ± 11	−116 ± 18	337 ± 7
LMST_HVS17	J085623.74+211322.3	134.09893	21.222872	0.078	1.0	8.7	−8.7	−0.3	0.6	−292 ± 15	−50 ± 13	−132 ± 5	325 ± 17
LMST_HVS18	J173650.63+060814.4	264.21098	6.1373510	0.217	0.4	7.6	−7.6	0.2	0.1	−313 ± 5	−17 ± 32	−92 ± 19	329 ± 5
LMST_HVS19	J224207.91+072808.3	340.53297	7.4689990	0.316	0.8	7.9	−7.8	0.6	−0.5	−184 ± 23	−253 ± 4	92 ± 29	329 ± 8
LMST_HVS20	J091849.92-005331.5	139.70801	−0.892091	0.077	0.5	8.2	−8.2	−0.3	0.2	−202 ± 2	−239 ± 18	76 ± 2	322 ± 14
LMST_HVS21	J122723.65+482136.1	186.84858	48.360029	0.033	0.9	8.2	−8.2	0.2	0.8	298 ± 26	−113 ± 5	−43 ± 22	323 ± 22
LMST_HVS22	J124330.95+423119.9	190.87898	42.522216	0.077	1.5	8.4	−8.2	0.3	1.5	103 ± 9	−260 ± 16	−142 ± 18	315 ± 7
LMST_HVS23	J121437.93+542522.9	183.65808	54.423052	0.051	1.2	8.4	−8.4	0.4	1.1	302 ± 29	−85 ± 9	14 ± 22	316 ± 26
LMST_HVS24	J212028.30-013323.4	320.11794	−1.556502	0.085	1.1	7.4	−7.4	0.7	−0.6	−231 ± 25	−164 ± 4	−125 ± 42	312 ± 33
LMST_HVS25	J080608.76+063349.8	121.53652	6.5638360	0.077	1.9	9.5	−9.5	−1.0	0.6	−170 ± 6	−176 ± 7	185 ± 64	312 ± 33
LMST_HVS26	J065436.50+170313.8	103.64375	17.053856	0.700	0.2	8.2	−8.2	−0.0	0.0	−273 ± 11	120 ± 4	41 ± 4	302 ± 9
LMST_HVS27	J102757.74+090030.0	156.99059	9.008337	0.090	0.7	8.3	−8.2	−0.3	0.6	−525 ± 35	−154 ± 4	−89 ± 3	555 ± 34
LMST_HVS28	J120758.23+093231.9	181.99265	9.542214	0.050	0.8	8.0	−8.0	−0.2	0.7	−62 ± 4	−443 ± 26	−15 ± 4	447 ± 25

Note. r_{gc} is the galactocentric distance; (x, y, z, V_x, V_y, V_z) are the 6D Galactic phase-space coordinates; V_{gt} is the total (space) velocity in the Galactic rest frame.

appropriate lines for calibration, including the calcium Ca II H and K lines at, respectively, 3933 Å and 3968 Å and the near-infrared (near-IR; Ca II triplet at 8498 Å, 8542 Å, and 8662 Å). The mean RV errors for all spectra were less than 10 km s^{-1}.

Among our data set of 28 promising HVSs, 5 also have SDSS RV measurements. For the latter stars, we found reasonable consistency in the RV results. The residual standard deviation (σ) was 16.8 km s^{-1} when comparing our RV results with the SDSS DR9 values, and $\sigma = 29.7$ km s^{-1} when comparing the LAMOST 1D pipeline results with the SDSS data. This also implies that our IRAF reduction is more reliable than the LAMOST 1D pipeline results. Below (e.g., in Section 4), we compare the properties of our candidate HVSs in the context of literature-based determinations, where available, in more detail.

Note that a well-known, hyper-runaway B-type star (HIP 60350; see also Maitzen et al. 1998; Tenjes et al. 2001; Irrgang et al. 2010), is also included in our initial sample catalog (LAMOST designation: J122229.60+404935.5; see the top panel of Figure 1). This star's RV is 248 ± 13 km s^{-1} based on the LAMOST 1D pipeline and 257 ± 8 km s^{-1} as derived from our IRAF results. This is in agreement with Irrgang et al. (2010), who found a barycentric RV of $v_{\rm rad} = 262 \pm 5$ km s^{-1}, based on a high-resolution optical echelle spectrum.

3.2. Distance Derivation

To obtain the six-dimensional (6D) phase-space coordinates of the HVS candidates, we first adopted the photometric parallax relations of Ivezić et al. (2008) to calculate the candidates' absolute r-band magnitudes, M_r. For objects with $0.2 < (g - i) < 4.0$ mag, we used

$$M_r(g - i, [\mathrm{Fe/H}]) = M_0 + \Delta M_r, \quad (1)$$

where ΔM_r and M_0 are given by, respectively, Equations (A2) and (A7) of Ivezić et al. (2008). Where available, we used the [Fe/H] values derived by the LAMOST pipeline. For objects without LAMOST metallicity determinations, photometric metallicities were adopted based on Equation (4) of Ivezić et al. (2008), for $0.2 < (g - r) < 0.6$ mag and $0.8 < (u - g) < 1.3$ mag. For stars that did not meet either of these color criteria, but which had $(r - i)$ colors in the range $0.1 < (r - i) < 1.6$ mag, a "bright" photometric parallax relation based on Equation (2) of Jurić et al. (2008) was used.

To derive the appropriate extinction corrections, we used the Rayleigh–Jeans color-excess method (Majewski et al. 2011), which estimates reddening values on a star-by-star basis using a combination of near- and mid-IR data from the Two Micron All-Sky Survey's (2MASS) point source catalog and the *WISE* catalog. Specifically, we used data in the H and *WISE* $W2$ (4.6 μm) bands:

$$A(K_s) = 0.918\{H - [4.6\ \mu\mathrm{m}] - (H - [4.6\ \mu\mathrm{m}])_0\}. \quad (2)$$

We adopted $(H - 4.6\ \mu\mathrm{m})_0 = 0.05$ mag (Zasowski et al. 2013) and $E(J - K_s) = 1.5A_{K_s}$ (Indebetouw et al. 2005).

To avoid reddening overcorrections of halo targets, we used the (Schlegel et al. 1998, hereinafter SFD) reddening maps as upper limit to the reddening toward stars in fields at Galactic latitudes $|b| \geqslant 16^\circ$ (see Zasowski et al. 2013), adopting

$$A_{K_s} = 0.302E(B - V)_{\rm SFD}, \quad (3)$$

as long as the $E(J - K_s)$ value calculated based on the 2MASS and *WISE* data was greater than 1.2× the SFD-derived value (Zasowski et al. 2013). The visual extinction A_V can then be obtained from $A_{K_s}/A_V = 0.118$ (Cardelli et al. 1989). For negative A_{K_s} values, we adopted the reddening values from the integrated SFD maps. We derived the r-band extinction, A_r, using $A_r/A_V = R_r/R_V = 0.8$, where $R_r = 2.31$ is given by Yuan et al. (2013) and $R_V = 3.1$ (Fitzpatrick 1999).

The distances thus derived from the de-reddened r-band distance modulus, combined with the positions of our 28 HVS candidates in 6D phase space, are sufficiently accurate and reliable to support our identification of these objects as genuine HVSs. We illustrated this in Section 3.1, where we discussed the properties of the highest-velocity star in our sample in the context of our full database of observed and derived parameters. In Section 4, we provide a number of examples of candidate stars whose spectra exhibit features as expected from their designations in the literature.

3.3. Spatial Velocity Calculations

We converted the RV, distance, and proper motions of each HVS candidate to V_x, V_y, and V_z in the (Cartesian) Galactic coordinate system centered on the GC, where the x-axis points to the direction opposite to that of the Sun, the y-axis is aligned with the direction of Galactic rotation, and the z-axis points toward the North Galactic Pole. The Sun is located at $x = -7.8$ kpc (McMillan & Binney 2010). The velocity of the local standard of rest (LSR) is set at 220 km s^{-1}, and the motion of the Sun with respect to the LSR is $(U_0, V_0, W_0) = (11.1, 12.24, 7.25)$ km s^{-1} (Schönrich & Binney 2009). We used the Markov Chain Monte Carlo technique to extract the U, V, and W components of all candidates from the normally distributed parameter space of RV, distance, and proper motions. We estimated the typical uncertainty associated with the RVs based on LAMOST spectra at 13 km s^{-1} (Luo et al. 2012). The resulting photometric distance accuracy is then approximately 10%, assuming rms values of the absolute M_r magnitudes of approximately 0.05 mag (Ivezić et al. 2008) and photometric r-band magnitude uncertainties of ∼0.02 mag (York et al. 2000). The kinematic parameters pertaining to our 28 HVS candidates thus derived are included in Table 2.

4. CONCLUSIONS

In this Letter, we have reported the discovery of a sample of 28 HVSs selected from the LAMOST DR1, of which 12 objects are the most likely HVS candidates. Our sample of HVS candidates covers a much broader color range than the equivalent ranges discussed in previous studies and comprises the first and largest sample of HVSs in the solar neighborhood.

We have access to sufficiently accurate observed and derived parameters for all 28 HVS candidates to ascertain their nature as genuine HVSs. To further verify the reliability of the sample of 28 HVSs, we matched our candidates with other catalogs. We first checked their proper motions based on the PPMXL catalog (Roeser et al. 2010) and did not find any significant differences between the PPMXL and UCAC4 catalogs for these 28 HVSs. Two candidates in the New Luyten Two Tenths (NLTT) catalog (Luyten 1979a, 1979b), LMST_HVS3 and LMST_HVS6, have proper motions of $[\mu_\alpha \cos(\delta), \mu_\delta] = (-154.2, -359.1)$ mas yr^{-1} and $(-197.2, -384.9)$ mas yr^{-1}, respectively (Salim & Gould 2003). LMST_HVS3 is identified as a K-type star in the NLTT catalog, where it is catalogued as object 309–34; careful analysis of our LAMOST spectra also classifies it as a K dwarf star. (The nearest NLTT star is located at a projected distance of approximately 12′, so that there can be no confusion as to

Table 3
Distances and Derived Kinematic Parameters of the 28 HVS Candidates from the Literature

Name	R.A. (deg)	Decl. (deg)	$D_\odot$ (kpc)	V_x (km s^{-1})	V_y (km s^{-1})	V_z (km s^{-1})	V_{gt} (km s^{-1})	Ref.
LMST_HVS1	134.58293	15.064578	1462	−254	−283	− 9	381	1
LMST_HVS2	141.77954	24.464709	...	...	...	...	...	...
LMST_HVS3	115.63816	32.409389	...	...	...	...	...	...
LMST_HVS4	344.84410	26.402775	1329	57	319	592	675	1
LMST_HVS5	178.69142	52.588984	1010	444	−26	21	445	1
LMST_HVS6	127.38536	28.437039	...	...	...	...	...	...
LMST_HVS7	348.13358	26.844326	...	...	...	...	...	...
LMST_HVS8	209.88189	41.522689	1890 (714)	40 (28)	−571 (−19)	557 (357)	799 (359)	1 (2)
LMST_HVS9	206.58962	30.263401	2475	287	−436	−117	536	1
LMST_HVS10	165.53608	57.866742	130	167	126	−135	250	1
LMST_HVS11	340.43813	29.407892	...	...	...	...	...	...
LMST_HVS12	190.08345	45.549896	2468	611	−158	−30	632	1
LMST_HVS13	187.89571	42.793379	2378	493	−185	−84	534	1
LMST_HVS14	145.34323	−0.139505	1484 (1267)	−195 (−193)	−431 (−375)	−169 (−106)	503 (435)	1 (2)
LMST_HVS15	112.71130	29.536856	798	321	−24	−118	343	2
LMST_HVS16	189.17285	44.621092	...	...	...	...	...	...
LMST_HVS17	134.09893	21.222872	1031	−293	−52	−135	327	1
LMST_HVS18	264.21098	6.1373510	...	...	...	...	...	...
LMST_HVS19	340.53297	7.4689990	3658	−565	−830	−597	1169	1
LMST_HVS20	139.70801	−0.892091	1455 (596)	−157 (−199)	−523 (−263)	−244 (48)	599 (333)	1 (2)
LMST_HVS21	186.84858	48.360029	5099	1322	−1394	608	2015	1
LMST_HVS22	190.87898	42.522216	2422	129	−500	−86	524	1
LMST_HVS23	183.65808	54.423052	1204	292	−78	7	303	1
LMST_HVS24	320.11794	−1.556502	...	...	...	...	...	...
LMST_HVS25	121.53652	6.5638360	2415	−138	−220	187	320	1
LMST_HVS26	103.64375	17.053856	...	...	...	...	...	...
LMST_HVS27	156.99059	9.008337	1878	−1143	−494	−594	1380	1
LMST_HVS28	181.99265	9.542214	1698	−147	−1113	−263	1153	1

References: (1) Pickles & Depagne 2010; (2) Gontcharov et al. 2011.

our candidate HVS's nature on this basis.) We have double checked the spectral features of all 28 HVS candidates, none of which exhibit characteristics of white dwarfs or binary systems. LMST_HVS1 is also listed as a high proper-motion star [$\mu_\alpha \cos(\delta) = -20.8$ mas yr^{-1}, $\mu_\delta = -54.8$ mas yr^{-1}] in the catalog of stars with high proper motions (Ivanov 2008). For all three stars, the similarity of the proper motions indicates the reliability of our kinematic data.

Since the uncertainty in distance is the major contributor to the uncertainties in the derived total (space) velocities, we use additional available photometric distances from Pickles & Depagne (2010) and Gontcharov et al. (2011) to recalculate the total velocities of our sample of 28 HVSs. Based on these literature-based distances, the derived total velocities and (U, V, W) components in the Galactic rest frame are listed in Table 3, while the proper motions and RVs used are included in Table 1. The space velocities of the 28 candidates included in Table 3 suggest that the candidates we discovered are highly probable HVSs because of their intrinsically large proper motions and RVs.

The results reported here also highlight the great potential of discovering statistically large numbers of HVSs of different spectral types in LAMOST survey data. We will continue to perform further systematic HVS searches based on the LAMOST data; the resulting stellar samples will eventually enable us to better understand the nature of the HVSs themselves and ultimately constrain the structure of the Galaxy.

This work was supported by "973 Program" 2014 CB845702, the Strategic Priority Research Program "The Emergence of Cosmological Structures" of the Chinese Academy of Sciences (CAS; grant XDB09010100) and by the National Natural Science Foundation of China (NSFC) under grants 11373054, 11073038, 11073001, and 11373010. The Guoshoujing Telescope (LAMOST) is a National Major Scientific Project built by the CAS. Funding for the project has been provided by the National Development and Reform Commission. LAMOST is operated and managed by the National Astronomical Observatories, CAS.

REFERENCES

Brown, W. R., Geller, M. J., & Kenyon, S. J. 2009, ApJ, 690, 1639
Brown, W. R., Geller, M. J., & Kenyon, S. J. 2012, ApJ, 751, 55
Brown, W. R., Geller, M. J., Kenyon, S. J., & Kurtz, M. J. 2005, ApJL, 622, L33
Cardelli, J. A., Clayton, G. C., & Mathis, J. S. 1989, ApJ, 345, 245
Carlin, J. L., Lépine, S., Newberg, H. J., et al. 2012, RAA, 12, 755
Chen, L., Hou, J.-L., Yu, J.-C., et al. 2012, RAA, 12, 805
Cui, X., Zhao, Y., Chu, Y., et al. 2012, RAA, 12, 1197
Deng, L. C., Newberg, H. J., Liu, C., et al. 2012, RAA, 12, 735
Fitzpatrick, E. L. 1999, PASP, 111, 63
Gontcharov, G. A., Bajkova, A. T., Fedorov, P. N., & Akhmetov, V. S. 2011, MNRAS, 413, 158
Hills, J. G. 1988, Natur, 331, 687
Indebetouw, R., Mathis, J. S., Babler, B. L., et al. 2005, ApJ, 619, 931
Irrgang, A., Przybilla, N., Heber, U., Nieva, M. F., & Schuh, S. 2010, ApJ, 711, 138
Ivanov, G. A. 2008, KFNT, 24, 480
Ivezić, Ž., Sesar, B., Jurić, M., et al. 2008, ApJ, 684, 287
Jurić, M., Ivezić, Ž., Brooks, A., et al. 2008, ApJ, 673, 864
Kollmeier, J. A., Gould, A., Knapp, G., & Beers, T. C. 2009, ApJ, 697, 1543
Kollmeier, J. A., Gould, A., Rockosi, C., et al. 2010, ApJ, 723, 812
Leonard, P. J. T. 1991, AJ, 101, 562
Li, Y., Luo, A., Zhao, G., et al. 2012, ApJL, 744, L24

Liu, C., Deng, L. C., Carlin, J. L., et al. 2014, ApJ, submitted (arXiv:1404.4871)
Luo, A., Zhang, H., Zhao, Y., et al. 2012, RAA, 12, 1243
Luyten, W. J. 1979a, New Luyten Catalogue of Stars with Proper Motions Larger than Two Tenths of an Arcsecond, Vol. 1: +90 Degrees to +30 Degrees (Minneapolis: Univ. Minnesota Press)
Luyten, W. J. 1979b, New Luyten Catalogue of Stars with Proper Motions Larger than Two Tenths of an Arcsecond, Vol. 2: +30 Degrees to 0 Degrees (Minneapolis: Univ. Minnesota Press)
Maitzen, H. M., Paunzen, E., Pressberger, R., Slettebak, A., & Wagner, R. M. 1998, A&A, 339, 782
Majewski, S. R., Zasowski, G., & Nidever, D. L. 2011, ApJ, 739, 25
McMillan, P. J., & Binney, J. J. 2010, MNRAS, 402, 934
Moyano Loyola, G. R. I., & Hurley, J. R. 2013, MNRAS, 434, 2509
Napiwotzki, R., & Silva, M. D. V. 2012, MmSAI, 83, 272
Palladino, L. E., Schlesinger, K. J., Holley-Bockelmann, K., et al. 2014, ApJ, 780, 7
Pickles, A., & Depagne, É. 2010, PASP, 122, 1437
Prugniel, Ph., Soubiran, C., Koleva, M., & Le Borgne, D. 2007, ELODIE Library Version 3.1 (arXiv:astro-ph/0703658)
Roeser, S., Demleitner, M., & Schilbach, E. 2010, AJ, 139, 2440
Salim, S., & Gould, A. 2003, ApJ, 582, 1011
Schlegel, D. J., Finkbeiner, D. P., & Davis, M. 1998, ApJ, 500, 525
Schönrich, R., & Binney, J. 2009, MNRAS, 396, 203
Tenjes, P., Einasto, J., Maitzen, H. M., & Zinnecker, H. 2001, A&A, 369, 530
Tillich, A., Przybilla, N., Scholz, R.-D., & Heber, U. 2009, A&A, 507, L37
Tillich, A., Przybilla, N., Scholz, R. D., & Heber, U. 2010, A&A, 517, A36
Wang, B., & Han, Z. 2009, A&A, 508, L27
Yang, F., Carlin, J. L., Liu, C., et al. 2012, RAA, 12, 781
Yu, Q., & Tremaine, S. 2003, ApJ, 599, 1129
Yuan, H. B., Liu, X. W., & Xiang, M. S. 2013, MNRAS, 430, 2188
Zasowski, G., Johnson, J. A., Frinchaboy, P. M., Majewski, S. R., et al. 2013, AJ, 146, 81
Zhang, Y.-Y., Carlin, J. L., Yang, F., et al. 2012, RAA, 12, 792
Zhao, G., Zhao, Y.-H., Chu, Y.-Q., Jing, Y.-P., & Deng, L.-C. 2012, RAA, 12, 723
Zheng, Z., Carlin, J. L., Beers, T. C., et al. 2014, ApJL, 785, L23
York, D. G., Adelman, J., Anderson, J. E., Jr., et al. 2000, AJ, 120, 1579